

Simulating ice layer formation under the presence of preferential flow in layered snowpacks

Nander Wever^{1,2}, Sebastian Würzer^{1,2}, Charles Fierz², and Michael Lehning^{2,1}

¹ École Polytechnique Fédérale de Lausanne (EPFL), School of Architecture, Civil and Environmental Engineering, Lausanne, Switzerland.

² WSL Institute for Snow and Avalanche Research SLF, Davos, Switzerland.

Correspondence to: Nander Wever (wever@slf.ch)

Abstract. For physics based snow cover models, simulating the formation of dense ice layers inside the snowpack has been a long time challenge. Their formation is considered to be tightly coupled to the presence of preferential flow, which is assumed to happen through flow fingering. Recent laboratory experiments and modelling techniques of liquid water flow in snow have advanced the understanding of conditions under which preferential flow paths or flow fingers form. We propose a modelling approach in the one-dimensional, multi-layer snow cover model SNOWPACK for preferential flow that is based on a dual-domain approach. The pore space is divided into a part that represents matrix flow and a part that represents preferential flow. Richards equation is then solved for both domains and only water in matrix flow is subjected to phase changes. We found that preferential flow paths arriving at a layer transition in the snowpack may lead to ponding conditions, which we used to trigger a water flow from the preferential flow domain to the matrix domain. Subsequent refreezing then can form dense layers in the snowpack, that regularly exceed 700 kg m^{-3} . A comparison of simulated density profiles with bi-weekly snow profiles made at the Weissfluhjoch measurement site at 2536 m altitude in the Eastern Swiss Alps for 16 snow seasons showed that several ice layers that were observed in the field could be reproduced. However many profiles remain challenging to simulate. The prediction of the early snowpack runoff also improved under the consideration of preferential flow. Our study suggests that a dual domain approach is able to describe the net effect of preferential flow on ice layer formation and liquid water flow in snow in one-dimensional, detailed, physics based snowpack models, without the need for a full multi-dimensional model.

1 Introduction

Ice layers form a marked microstructural transition inside the snowpack (Fierz *et al.*, 2009). Their formation is generally considered to be tightly coupled to the presence of preferential flow in snow (Marsh and Woo, 1984; Pfeffer and Humphrey, 1998; Fierz *et al.*, 2009). Despite their often small vertical extent, (thin) ice layers may have a profound impact on large scale processes in a snowpack, such as liquid water, heat and vapour flow (Colbeck, 1991; Hammonds *et al.*, 2015). Many fields of study have addressed the issue of ice layers in snowpacks. Water may flow laterally over ice layers or crusts, which reduces travel times in catchments and has a significant impact on catchment scale hydrology; alternatively, preferential flow in snow may promote vertical percolation instead (Eiriksson *et al.*, 2013). Recent studies have demonstrated that the increased melt on the Greenland Ice Sheet during the last few decades lead to changes in the firn structure, particularly through the formation of

ice layers by percolating water in sub-freezing snow (*de la Peña et al.*, 2015). These ice layers can reach considerable vertical extents on the order of 1 m (*Machguth et al.*, 2016) and may reduce the storage capacity of melt water in the firm by making access to deeper firn layers more difficult. Subsequent melt events may thus be accompanied by much more efficient runoff, due to lateral flow over these ice layers (*Pfeffer et al.*, 1991). Ice layers can also have a profound impact on microwave emission from the snowpack, which is used in remote sensing retrieval algorithms (*Rees et al.*, 2010; *Roy et al.*, 2016). For rock stability of permafrost affected regions, the presence of ice layers near the base of the snowpack as well as inside the snowpack was found to prevent liquid water from reaching joints in the rocks, thereby improving rock stability (*Phillips et al.*, 2016). Ice layers in snowpacks also impact the access to food resources for wild life in snow covered areas (e.g., *Vikhamar-Schuler et al.* (2013)). Climate change projections of future increases in rain-on-snow events in high latitudes (*Ye et al.*, 2008), increased snow melt on ice sheets (*de la Peña et al.*, 2015) as well as more frequent melt events in alpine snowpacks (*Surfleet and Tullos*, 2013) show urgency to be able to determine how these changes affect the snowpack microstructure in the future.

For 1D snow cover models, whether they are physics based or simple, it is notoriously difficult to simulate the formation of ice layers. This can be understood as most models do not consider preferential flow, which is a crucial transport mechanism to allow downward propagating water flow in sub-freezing snow. Liquid water can thereby reach areas in the snowpack where the cold content is large enough to refreeze the percolating melt water and form ice layers (*Humphrey et al.*, 2012). In early attempts by *Colbeck* (1979) and *Marsh and Woo* (1985) to describe preferential flow in snowpack models, the water flow in snow is considered as a flow in multiple flow paths. In *Colbeck* (1979), flow paths are defined that differ in size and snowpack properties, which results in different percolation speeds in the individual snow paths when applying Darcy's law. In *Marsh and Woo* (1985), the snowpack is divided in flow paths of equal size and snowpack properties, but based on compartmented lysimeter measurements, it is determined how much of the total flux is transported in each of the individual flow paths. Both approaches never found widespread adoption, probably because they require a-priori specification of the flow path variability (*Marsh*, 1999). In *Katsushima et al.* (2009), a description of preferential flow for snowpack models is proposed where water in excess of a threshold in saturation (for example in ponding conditions inside the snowpack) is directly routed to the soil below the snowpack. This approach improved the prediction of snowpack runoff, but is not able to simulate the formation of ice layers due to percolating melt water in preferential flow channels, as the water in preferential flow is considered to have left the snow domain of the model. The fact that many snow models neglect preferential flow, even when they are used for hydrological studies where snowpack runoff is a primary process, may be justified for describing seasonal runoff characteristics (*Wever et al.*, 2014a). However preferential flow may be crucial for understanding the response of a snow cover on short, sub-daily time scales, for example during rain-on-snow events (*Katsushima et al.*, 2009; *Rössler et al.*, 2014; *Wever et al.*, 2014b; *Würzer et al.*, 2016a). Also for wet snow avalanche formation, the exact location at which liquid water starts ponding can influence snow stability (*Wever et al.*, 2016) and considering preferential flow may be important for the exact timing of when weak layers are reached by water. Snowpack models developed for avalanche warning purposes (*Brun et al.*, 1992; *Lehning et al.*, 1999) may therefore also benefit from a description of preferential flow processes in snow.

Multi-dimensional snow cover models have been developed to simulate preferential flow (*Illangasekare et al.*, 1990; *Hirashima et al.*, 2014), but those models simplified and neglected several snowpack processes (i.e., snow settling, snow mi-

crostructure evolution), meaning that they are not yet applicable to natural snowpacks. Furthermore, multi-dimensional snow cover models generally require more computational power, making them unsuitable for large scale deployment. However, those multi-dimensional model developments provide crucial insights that allowed for a parametrisation of a dual domain approach for preferential flow for the 1D, physics based, detailed SNOWPACK model (Bartelt and Lehning, 2002; Lehning et al., 2002a, 5 b), which we present in this study.

2 Dual Domain Implementation

To simulate preferential flow, we apply a dual domain approach as schematically shown in Fig. 1. The pore space is subdivided into a part that is involved in preferential flow, and a part that is representing matrix flow (labelled 1 in Fig. 1). For the construction of the domains and the exchange processes between both domains, we exploit recent results from laboratory and 10 model experiments as well as applying concepts from hydrological modelling. The water flow in the model is described for both the matrix and preferential flow domain by solving Richards equation for both domains sequentially at the commonly used SNOWPACK time step of 15 min. After solving Richards equation for the matrix domain, the exchange of water between the matrix and preferential flow domain is determined and vice versa. If the pressure head exceeds the water entry pressure head of the layer below (labelled 2 in Fig. 1) water moves from matrix to preferential flow (labelled 3 in Fig. 1). If the saturation in 15 the preferential flow path exceeds a threshold (labelled 4 in Fig. 1), water moves back to the matrix domain (labelled 5 in Fig. 1). Only the matrix part is allowed to undergo phase changes and ice layers form when water moves back from preferential flow to matrix flow and refreezes. Preferential flow remains always in the liquid phase. Refreezing of preferential flow water is mimicked by moving water from preferential flow to the matrix flow domain (labelled 6 in Fig. 1). Below, the water exchange processes are described in more detail.

20 2.1 Defining the Dual Domains

For the dual domain approach, the pore space is subdivided in a matrix and preferential flow domain (denoted with 1 in Fig. 1). For soils, the relative area involved in preferential flow is often found to be a function of the ratio of system influx rate over saturated hydraulic conductivity (Glass et al., 1989a, b) for a given soil texture. In the experimental data on snow presented by Katsushima et al. (2013), a more pronounced dependence of the preferential flow area with grain size is found, rather than with 25 the system influx rate. We illustrate their experimental results graphically in Fig. 2. Whereas the grain size shows a distinct pattern of smaller preferential flow area for larger grain sizes, the system influx rate showed a rather ambiguous pattern, where increased influx did not always lead to a larger preferential flow area. The grain sizes used in their experiments span over typical ranges found in natural snowpacks and this dependence is important to take into account. It also has to be noted that the infiltration rates in their experiments exceed typical values in natural conditions. We therefore decided to determine the

dependence of preferential flow area on grain size using the lowest experimental infiltration rate only. A fit to this selection of the data (see Fig. 2) provides the following expression for the preferential flow area (F):

$$F = 0.0584r_g^{-1.109}, \quad (1)$$

where F is the preferential flow area fraction (-), and r_g is the grain radius (mm). The matrix flow domain is accordingly defined as $(1 - F)$. For fine grained snow ($r_g \approx 0.12$ mm), *Katsushima et al.* (2013) did not observe preferential flow, in contrast with the snow samples with $r_g \approx 0.21$ mm and larger. However, typically most parts of the snowpack consist of larger grains than the smallest grain size used in the experiments. Thus, to provide a continuum description of the matrix and preferential flow regime, Equation 1 is used for all grain sizes. For numerical stability, F is limited between 0.01 and 0.90. Generally grain size increases over time in snow, and this may occasionally lead to a situation where the preferential flow area in the next SNOWPACK time step is reduced below the required one to accommodate for the liquid water present in the preferential flow domain. We therefore additionally ensure that F is large enough to contain all present preferential flow water.

For both domains, the relationship between pressure head and liquid water content (LWC) is described by the van Genuchten parametrisation for snow as experimentally determined by *Yamaguchi et al.* (2012). For the matrix flow domain, the saturated LWC is scaled by $(1 - F)$ and for the preferential flow domain by F . Furthermore, we determine the residual water content for the matrix flow domain using the approach described in *Wever et al.* (2014a), while setting it to 0 for the preferential flow domain. Saturated hydraulic conductivity is parametrised using the parametrisation for permeability proposed by *Calonne et al.* (2012).

2.2 Water Exchange Between Matrix and Preferential Flow Domain

All liquid water input (snow melt, rainfall, condensation) is added to the matrix flow domain. A prerequisite for the formation of an unstable wetting front (i.e., flow fingering) is that the system influx rate is below the saturated hydraulic conductivity of the medium (*DiCarlo*, 2013), which is generally fulfilled in snow (*Katsushima et al.*, 2013). In order to initiate preferential flow, we use the concept that preferential flow paths form when the pressure head in the matrix flow domain exceeds the water entry pressure of the layer below. This was found to be the case in laboratory experiments (*Katsushima et al.*, 2013; *Avanzi et al.*, 2015) and was successfully exploited in numerical modelling to initiate preferential flow (*Katsushima et al.*, 2009; *Hirashima et al.*, 2014). The water entry pressure h_{we} (m) can be expressed as a function of grain radius according to *Katsushima et al.* (2013):

$$h_{we} = 0.0437(2r_g) + 0.01074. \quad (2)$$

One important condition to reach the water entry pressure is water ponding on a microstructural transition inside the snowpack (*Hirashima et al.*, 2014; *Avanzi et al.*, 2015). This is denoted with 2 in Fig. 1. To achieve the high LWC value observed in experiments (*Avanzi et al.*, 2015), we use the geometric average to calculate the hydraulic conductivity between snow layers (*Wever et al.*, 2015). In our implementation, the amount of water in the matrix part in excess of the threshold corresponding to

the water entry pressure of the layer below, is moved to the preferential flow domain in the layer below (denoted with 3 in Fig. 1). A capillary overshoot condition was found in snow (Katsushima *et al.*, 2013), which means that the capillary pressure in the ponding layer decreases again after preferential flow forms. This increases the liquid water content in the preferential flow paths and to mimic this effect, we allow more water to flow from matrix flow to preferential flow once the threshold is exceeded than only the amount of water above the threshold. If after the water in excess of the threshold is moved and the saturation (i.e., ratio of water volume to pore volume) in the layer in the matrix domain is still higher than the saturation in the layer below in the preferential flow domain, the saturation is equalized by an equivalent water flow with the following approach. Equal saturation in a specific layer with index i in the matrix domain and a layer with index j in the preferential flow domain can be expressed as:

$$10 \quad \frac{\theta_m^i - \theta_{r,m}^i}{\theta_{s,m}^i - \theta_{r,m}^i} = \frac{\theta_p^j - \theta_{r,p}^j}{\theta_{s,p}^j - \theta_{r,p}^j}, \quad (3)$$

Where the subscripts m and p denote the matrix and preferential flow domain, respectively, θ is the LWC ($\text{m}^3 \text{m}^{-3}$), θ_r is the residual LWC ($\text{m}^3 \text{m}^{-3}$) and θ_s is the saturated LWC ($\text{m}^3 \text{m}^{-3}$). In the model, layers are counted from below, such that equalizing saturation between the matrix domain in the layer above and the preferential flow domain in the layer below corresponds to $j = i - 1$.

15 Given layer thicknesses L_m^i and L_p^j for the layers in the matrix flow and preferential flow domain, respectively, the total LWC in the matrix and preferential flow layer is defined as:

$$\theta_{\text{tot}} = \theta_m^i L_m^i + \theta_p^j L_p^j \quad (4)$$

Under the requirement of an equal degree of saturation for a given total LWC, we can solve Eq. 3 for θ_m^i :

$$20 \quad \theta_m^i = - \frac{(\theta_{r,m}^i \theta_{s,p}^j - \theta_{r,p}^j \theta_{s,m}^i) L_m^i + (\theta_{r,p}^j - \theta_{s,p}^j) \theta_{\text{tot}}}{(\theta_{s,m}^i - \theta_{r,m}^i) L_m^i + (\theta_{s,p}^j - \theta_{r,p}^j) L_p^j}, \quad (5)$$

after which θ_p^j can be found by applying Eq. 4.

Additionally, if the saturation in the matrix domain exceeds the saturation of the preferential flow domain in a snowpack layer, saturation is equalized using Eq. 5, with $i = j$ and consequently $L_m^i = L_p^j$. This is motivated by the fact that once snow is wet, no horizontal gradients in pressure head are expected to be present in a snow layer, and thus, following the Van Genuchten water retention curve, the saturation of the matrix domain is equal to the saturation of the preferential flow domain.

25 Conceptually, water will leave the preferential flow domain and enter the matrix domain if the pressure head inside the preferential flow domain exceeds the water entry pressure of the dry snow around the preferential flow path. This procedure was able to simulate water spreading on microstructural transitions in the multi-dimensional snow model by Hirashima *et al.* (2014). However, in our study, this approach rarely succeeded in forming ice layers, as the condition is rather seldom met. This fact can be interpreted in light of the physics behind preferential flow. It was demonstrated that an overshoot condition exists in flow fingers, which means that the tip of a flow finger shows marked higher saturation than the tail. This flow behaviour cannot be described by Richards equation (DiCarlo, 2013), although Richards equation continues to provide a correct description

above and below the wetting front. The reason why the condition worked in *Hirashima et al.* (2014) may be due to the fact that the simulations involved high water influx rates, much higher than experienced in natural snowpacks. This would increase the amount of water accumulating on the capillary barrier when liquid water flow over the transition is slower than the water flux arriving from above. In the absence of a solution for this problem (*DiCarlo*, 2013), we simply apply a threshold in saturation

5 (Θ_{th}) of the preferential flow domain (denoted with 4 in Fig. 1). Once this threshold is exceeded, water will flow back to the matrix domain (denoted with 5 in Fig. 1). In our approach, we first move as much water as freezing capacity is available in the matrix domain. If after this approach the threshold is still exceeded, we additionally equalize the saturation in the specific layer in the matrix and preferential flow domain, using Eq. 5. For the lowest snow layer above the soil, the saturation is always equalized between the matrix and preferential flow domain, regardless of whether the saturation threshold is exceeded

10 or not. This suppressed spiky snowpack runoff behaviour. In soil layers, preferential flow is ignored by setting the hydraulic conductivity for the preferential flow domain to 0 and the preferential flow area to 2 %.

2.3 Refreezing Preferential Flow

In our approach, water in the preferential flow domain is not considered for phase changes. However, in reality preferential flow is known to refreeze, even forming ice structures in the shape of flow fingers inside the snowpack (*Kattelmann*, 1985; *Marsh*, 1988; *Fierz et al.*, 2009; *Williams et al.*, 2000). For simplicity, we currently do not consider microstructural changes due to preferential flow, although they may have a strong effect on the water flow in snow. Grain growth and subsequent reduction of capillary forces as well as ice columns may increase the efficiency of the preferential flow paths considerably.

15

For the thermal effects, we first describe the heat flux between the preferential flow part and the matrix part by assuming a pipe with radius r (m) at melting temperature T_0 (K) in the middle of a 1 m^2 snowpack at temperature T_e (K) (see Fig. 3). If we assume that the horizontal temperature gradient inside the snowpack is linear, then the temperature T_e is found at a radius R^* (m) such that surface areas A_1 (m^2) and A_2 (m^2) are equal. We can then approximate Fourier's law for heat flow for the heat flux between the preferential flow and matrix domain ($Q_{H,p \rightarrow m}$, $\text{J m}^{-1} \text{ s}^{-1}$) as:

20

$$Q_{H,p \rightarrow m} = \kappa \frac{\partial T}{\partial x} \approx \kappa \frac{(T_e - T_0)}{\left(\sqrt{\frac{1+F}{2\pi}} - \sqrt{\frac{F}{\pi}}\right)} \quad (6)$$

The volumetric content that needs to be transferred from the preferential domain to the matrix domain (denoted with 6 in Fig. 1), in order to satisfy the refreezing capacity provided by the heat flux $Q_{H,p \rightarrow m}$ over the outer area of the preferential flow path can be subsequently expressed as:

25

$$\Delta\theta_{w,p \rightarrow m} = N\pi FL_e Q_{H,p \rightarrow m} \Delta t \quad (7)$$

where L_e is the latent heat associated with freezing ($3.34 \cdot 10^5 \text{ J kg}^{-1}$) and N is a factor describing the effect of multiple flow paths forming area F . Often, numerous flow paths can be identified per square meter of snowpack, as for example found in a field study by *McGurk and Marsh* (1995). They report a flow path density between roughly 100 to 300 per m^2 . However, this number is not necessarily representative for the number of flow paths actively and concurrently transporting water, as often

30

new preferential flow paths form in subsequent melt cycles (Schneebeli, 1995). Albert *et al.* (1999) found only 3 preferential flow paths per m² during the first wetting of a previously sub-freezing snowpack. When more flow paths are present, the energy exchange will be more efficient. Additionally, the gradients with the surrounding snow will be larger. We use N as a tuning parameter in the model related to the number of flow paths per m².

5 3 Data and Methods

3.1 Data

We simulate 16 subsequent snow seasons (2000-2015) for the Weissfluhjoch (WFJ) measurement site, located at 2536 m altitude in the Eastern Swiss Alps. For this site, a dataset of bi-weekly snow-profiles made in close vicinity (<25m) of the meteorological station used to drive the SNOWPACK model in this study is available (WSL Institute for Snow and Avalanche Research SLF, 2015; Wever *et al.*, 2015). The snow profiles contain information about grain size and type, judged by the observer using a magnifying glass, as well as snow density in sections of typically 20-50 cm height and snow temperature. Melt-freeze crusts (i.e., parts of the snowpack that have been wet and froze again), as well as ice layers are explicitly marked as such in the profiles. Ice lenses (i.e., non continuous ice layers) are not marked as an ice layer, but are reported in a separate remark. As subsequent snow profiles need to be made in undisturbed snow, they also sample spatial variability in addition to the temporal evolution. Furthermore, judging whether a specific layer is a crust or an ice layer is also partly subjective. This is also indicated in the data: sometimes the same layer is not identified similarly in subsequent snow profiles, although this may also indicate spatial variability. To account for spatial variability at the measurement site, we select the highest modelled dry snow density within a range of 20 cm above or below an observed ice layer, when comparing simulated and observed ice layers.

For validating the snowpack runoff simulated by the model, we use the snow lysimeter data from a 5 m² lysimeter, as described in Wever *et al.* (2014a). In that paper, it was discussed that a discrepancy between measured and modelled runoff is particularly present at the beginning of the melt season, and involves the first ca. 5 % of seasonal snowpack runoff. Here, we consider the measured snowpack runoff for the period March 1 to May 31 only, and particularly focus on the first 20 mm w.e. runoff from the snowpack. This period corresponds to the onset of snowpack runoff, while preventing that the statistics are dominated by the main melt period. We additionally exclude lysimeter data from snow season 2000 and 2005 from the analysis, due to suspected problems with the lysimeter in these seasons (Wever *et al.*, 2014a).

3.2 Methods

3.2.1 Model Setup

The simulation setup of the SNOWPACK model for WFJ is equal to the snow-height driven simulations in Wever *et al.* (2015), in which new snow fall amounts are determined from increases in measured snow height. This ensures a simulation that closely follows the measured snow height, which will enable a correct comparison of simulated and observed snow profiles. Ice layers

observed in the field can range from a few mm to a few cm and up to 1 m in firn on the Greenland Ice Sheet (Fierz *et al.*, 2009; Machguth *et al.*, 2016). To reduce computational costs, the SNOWPACK model applies an algorithm to merge elements when they exhibit similar properties. In default setting, this procedure typically maintains the layer spacing around 1.5 to 3 cm, except for certain special cases, like buried surface hoar or ice layers inside the snowpack, which should be maintained irrespective of their thickness. This means that in default setup, with a typical layer spacing of 1.6 cm, the formation of ice layers is coupled to relatively thick layers compared to ice layers found in natural alpine snowpacks. Forming thinner ice layers requires less water and energy to refreeze. We therefore performed high resolution simulations where we lower the threshold above which no merge is allowed from 1.5 cm to 0.25 cm. Further, for the high resolution simulations, we initialize new snow layers during snowfall in steps of 0.5 cm, instead of the default value of 2 cm. This lead to a typical layer spacing of 0.45 cm. Results presented here are with the high resolution simulations, although we discuss the performance of the default resolution as well. Simulations with matrix flow only took on average 2.3 min per simulated year to complete on a typical desktop PC, using the default SNOWPACK settings. The dual domain approach, which requires solving Richards equation twice, increased the computation time to 8.0 min per year. The high resolution simulations, which we show here, took 71 min per year to complete.

Densities of ice layers in the field can vary over a wide range. For example, Marsh and Woo (1984) reports a range from 630 to 950 kg m⁻³, which makes it ambiguous to determine above which threshold of modelled dry snow density a layer should be considered an ice layer. In the default setup, a layer with a dry snow density exceeding 700 kg m⁻³ is considered an ice layer by the SNOWPACK model. However, we apply different thresholds here to verify the sensitivity of the choice of threshold on the results. Indeed, it may be that simulated layers cannot reach the density of observed, thin, ice layers due to their larger vertical extent in the model.

20 4 Results

4.1 Parameter Estimation

In the preferential flow formulation we propose, two tuning parameters are left: the threshold in saturation of the preferential flow domain (Θ_{th}), above which water will flow back to the matrix part, and a parameter related to the number of flow paths per m² (N). To determine an optimal set of parameters, a sensitivity study was carried out. For Θ_{th} , values from 0.02 to 0.16 in steps of 0.02 were used and for N , values 0, 0.2, 0.4, 0.6, 0.8, 1.0, 2.0, 3.0, 4.0, 5.0 were used.

Fig. 4 shows the probability of detection POD (i.e., the ratio of observed ice layers that are reproduced by the model over the total number of observed ice layers) for different thresholds that define a modelled ice layer, as a function of both tuning parameters. When ice layers are defined by higher densities, the POD decreases. Highest POD is achieved for no or minor freezing (i.e., small values for N), and a saturation in the preferential flow path around 0.1. The non-linear relationship in Fig. 4 arises from the delicate balance of refreezing water that is not able to percolate deeper and the amount of ponding possible at microstructural transitions, required for water to move back to the matrix domain in order to freeze as an ice layer or lens. For snowpack runoff, highest scores in terms of r^2 , RMSE or the arrival date of the first 20 mm w.e. are generally achieved with refreezing and low thresholds in saturation of the preferential flow domain (see Fig. 4). Both slow down the progression

of preferential flow water. It seems difficult to find a set of parameters that will maximize both the reproduction of ice layers, as well as snowpack runoff simulations. Nevertheless, even with optimal settings for the formation of ice layers, the early stage of snowpack runoff (i.e., the passage time of the first 20 mm w.e. of runoff) is better reproduced than without considering preferential flow.

5 After executing all 80 SNOWPACK simulations for the sensitivity study, ranks were determined for the POD of ice layers, using 700 kg m^{-3} as density threshold for ice layers, and the r^2 value for hourly snowpack runoff. The combination of both parameters that provides the lowest sum of the ranks for ice layer detection and snowpack runoff was considered the optimal combination of coefficients. This procedure gave $\Theta_{\text{th}} = 0.1$ and $N = 0$ and $\Theta_{\text{th}} = 0.08$ and $N = 0$ for the normal and high resolution simulations, respectively, as optimal combination of tuning parameters and this set of parameters will be used for
10 the results. Interestingly, it implies that for ice layer formation, refreezing of preferential flow should be ignored (i.e., $N = 0$).

4.2 Example Snow Season

Fig. 5 illustrates the difference in simulated snow density between a simulation with only Richards equation and Richards equation including preferential flow at high resolution for snow season 2012. Similar figures for the other simulated snow seasons are shown in the Online Supplement. The overall density distribution is similar in both simulations, but only with
15 preferential flow, ice layers are formed. The location is in good agreement with observations of ice layers and crusts observed in the snow profiles in the field. Fig. 6 shows detailed simulation output for the period in the beginning of March 2012 and the upper part of the snowpack only. The distribution of liquid water is showing that the preferential flow (Fig. 6b) is percolating ahead of the matrix flow (Fig. 6a). This partly is due to the absence of phase changes for water in preferential flow, but also due to the lower area, and thereby lower value for θ_s , such that hydraulic conductivity increases faster with increasing LWC.
20 In contrast to matrix flow, preferential flow reaches areas where the snowpack is still below freezing (Fig. 6c).

Ponding at microstructural interfaces is occurring in both the matrix and the preferential flow domain. In the example, a jump in snow density (Fig. 6d) and grain radius (Fig. 6e) around 165 cm and 210 cm in the snowpack mark the layers where water accumulates, refreezes and forms ice layers (Fig. 6d,f). Solving Richards equation twice (for both domains) appears to be able to identify those layers. Refreezing locally increases the snow temperature to melting temperature (Fig. 6c). Initially,
25 the model identifies refreeze inside the snow layer and marks the layer as a melt-freeze crust. Once dry snow density exceeds 700 kg/m^3 , the layer is marked as an ice layer (Fig. 6f). Note that Fig. 6e shows that most of the snowpack consists of grain sizes for which preferential flow was observed in the experiments by *Katsushima et al.* (2013). The smallest grain size class from those experiments, for which no preferential flow was observed, is only found in the new snow layers during snowfall (black coloured areas), after which metamorphism rapidly increases grain size to regimes for which preferential flow was
30 observed. This justifies the application of Eq. 1 for the full range of grain size in the model.

In addition to preferential flow, ice layers can also form by surface processes. For example, rainfall in November 2003 in a sub-freezing snow cover formed an ice layer at the surface and this ice layer was subsequently observed during the rest of the 2004 snow season (see Fig. S5 in the Online Supplement). This layer is not reproduced in the SNOWPACK model. Firstly, the model did not recognize the precipitation as rainfall due to the low air temperature during the event. Second, even when

the model was forced to interpret the precipitation as rainfall, the ice layer did not form at the surface. The model solves for the heat and water flow sequentially in a 15 min. time step, whereas the formation of an ice layer during rainfall is occurring on shorter time scales. Furthermore, we hypothesize that rain droplets probably freeze directly upon contact with the snow surface, creating an ice layer locally at the surface, whereas the SNOWPACK model considers the rainfall as an incoming flux in the top layer. When the available energy for freezing is not sufficient to freeze the full depth of the top layer in the model, an ice layer is not formed. In reality, the surface ice layer is possibly even hindering water entry to deeper layers, which may thicken the surface ice layer. This particular ice layer in 2004 has been excluded in further analysis.

4.3 Density Profiles

Fig. 7 shows the observed snow density distribution in all snow profiles from snow seasons 2000-2015, typically representing vertical sections of 20-50 cm and sometimes smaller sections. The distribution of snow density for these sections is reproduced well by the simulations, although the spread in simulated snow density is lower than the observed spread. All simulations provide very similar snow density distributions. The r^2 value between observed and simulated density in the measurement sections is highest ($r^2=0.74$) for the simulations with Richards equation only and in *Wever et al. (2015)*, it is shown that the temporal evolution and vertical distribution of snow density is in good agreement with measured snow density. With preferential flow, the r^2 value reduces to 0.71. This reduction in model performance when using preferential flow is also confirmed when using Willmott's index of agreement (*Zambrano-Bigiarini, 2014; Willmott, 1981*), which was determined to be 0.84 and 0.83 for simulations with Richards equation only and simulations with preferential flow, respectively. Nevertheless, the simulations with preferential flow are maintaining the overall snowpack density profile generally well and the reduction in r^2 value may be attributed to the fact that calibration of snow settling functions was not performed considering the preferential flow model. Another reason may be that with preferential flow, more water is moved downward and less water can refreeze in matrix flow in the upper snow layers. It may be argued that an underestimation of snow settling can be compensated for by an overestimation of refreezing water. In any case, the simulations with preferential flow stand out when looking at the highest snow density simulated in a layer within ± 20 cm of an observed ice layer. In this case, much higher snow densities are found in individual layers under consideration of preferential flow.

As the manual snow density measurements in the field represent much larger vertical sections (20-30 cm), these measurements cannot be used to verify the much higher resolution (1-2 cm or less) simulated densities on that scale. Time series using other measurement techniques, as for example snow micro penetrometry (*Schneebeli and Johnson, 1998*) or measuring volume and mass of excavated ice layers (*Watts et al., 2016*), may assist in a more in-depth model verification in the future.

Fig. 8 shows the POD for different dry snow density thresholds that define an ice layer in the simulations. The POD decreases with increasing threshold from 0.44 for 400 and 500 kg m^{-3} to 0.10 for a threshold of 800 kg m^{-3} for the high resolution simulations. When comparing with field observations, it is important to note that it is not clear which density should be assigned to a layer that an observer would denote as an ice layer. The probability of null detection, which in this case is defined as the percentage of simulated profiles correctly simulating the absence of ice layers in the full profile is above 50 % for an ice layer definition threshold of 600 kg m^{-3} in high resolution simulations. In normal resolution simulations, the probability of null

detection is higher. The bias, which is the ratio of the number of simulated ice layers over the number of observed ice layers, is generally below 1. This indicates a slight underestimation of the frequency of ice layers in both high and normal resolution simulations. It shows that our approach is neither largely overestimating nor underestimating the presence of ice layers inside the snowpack. The false alarm rate indicates that around half of the ice layers that are simulated do not find a correspondence in the observed snow pits. The results illustrate the general difficulty of observing ice layers with often small vertical extent in the field and reproducing those ice layers in the model due to a delicate interaction between water flow and the ice matrix. However, the results also indicate that the model is able to capture a significant proportion of ice layers that formed in natural snowpacks, while maintaining the overall snowpack structure well. In contrast, simulations with Richards equation only generally do not reproduce any layer with a dry snow density exceeding 600 kg m^{-3} . The prediction bias is correspondingly below 0.20 even for low thresholds of 400 kg m^{-3} for defining an ice layer. This indicates that the failure of reproducing ice layers in those type of simulations cannot be resolved by choosing low thresholds, but that preferential flow seems to be a crucial process to simulate the formation of ice layers.

4.4 Snowpack Runoff

In addition to ice layer formation, snowpack runoff is also strongly impacted by preferential flow. For rain-on-snow events at the WFJ measurement site, Würzer *et al.* (2016b) found an improvement in r^2 from 0.52 for Richards equation only to 0.68 for the dual domain approach. Interestingly, Fig. 9 shows that for the melt period, there is no consistent difference between r^2 values for daily and hourly snowpack runoff whether or not preferential flow is considered. On average both simulations have equal r^2 values of 0.81 and 0.90 for hourly and daily snowpack runoff, respectively. However, as already noted in Wever *et al.* (2014b), the effect of neglecting preferential flow on seasonal time scales may be very limited. In that study, particularly the first arrival of melt water was noticeably underestimated when only considering matrix flow with Richards equation. As illustrated in Fig. 10, the arrival time of the first 20 mm w.e. in the melt season is much better reproduced by the dual domain approach. The time difference between the arrival date of the first 20 mm w.e. changes from 7.7 days too late for the Richards equation model to 2.9 days too early in the dual domain approach. Generally, the average time difference between modelled and measured first 10 mm w.e. cumulative snowpack runoff is even more negative than the average time difference for 20 mm w.e. cumulative runoff. This suggests that particularly earliest season snowpack runoff from preferential flow is overestimated in the simulations. The standard deviation of the time difference for 20 mm w.e. is slightly smaller for the preferential flow formulation than for the matrix flow only. The fact that the standard deviation is smaller indicates that yearly variability between observed and simulated runoff is smaller and that the model is apparently able to better explain yearly variability. In Würzer *et al.* (2016b) additional analysis of the role of preferential flow in producing snowpack runoff during rain-on-snow events shows that for these events, snowpack runoff is better reproduced using the dual domain approach.

Although considering preferential flow improved the snowpack runoff simulation, year-to-year variability in model performance is still large. The difference between simulations with or without preferential flow are often smaller than the year-to-year variability. For example, in melt season 2001 and 2010, r^2 values are low in both simulations and the difference between the simulations is smaller than the difference in r^2 values with other years. Explanatory factors for the year-to-year variability

in model performance for reproducing snowpack runoff were not found. Snowpack characterizing statistics, for example the observed number of ice layers or observed number of jumps in grain size and hardness, did not correlate significantly with r^2 for snowpack runoff or the arrival date. This is probably due to a combination of errors in meteorological forcing conditions, observer bias in the bi-weekly snow profiles, and the limited representativeness of the snow lysimeter. Its surface area of 5 m² may be considered too small to capture a representative area for snowpack runoff, such that randomness in the exact location where preferential flow paths form may influence the measurements (*Kattelmann, 2000*). Separating the individual errors appears to be difficult.

5 Discussion

In the implementation of the dual domain approach, we attempted to stay close to a physics based process description. Laboratory experiments and multi-dimensional snowpack models have provided crucial insights in the preferential flow and water ponding processes. However, the number of quantitative experimental studies is still limited and many aspects may be refined in further studies. The model uses four criteria to specify the dual domain approach: (1) the area involved in preferential flow, (2) a condition to move water from matrix flow to preferential flow, (3) a condition to move water from preferential flow to matrix flow, (4) a condition describing the refreezing process of preferential flow. Two calibrating coefficients, related to criterion 3 and 4 were used to optimize the simulations.

The area involved in preferential flow (condition 1) is currently parametrised with grain size only. Given observations from soil physics (e.g., *Glass et al. (1989b)*), a dependence on the water influx rate is to be expected. Currently, laboratory settings, or field experiments with rainfall generators have generally large water input rates of typically 20 mm/hour or more (*Singh et al., 1997; Katsushima et al., 2013; Würzer et al., 2016b*). It turns out to be difficult to have controlled, constant and spatially well distributed water input rates typically observed in nature (rainfall and melt rates of 1-5 mm/hour). The absence of studies at low water input rates makes the general validity of condition 1 we implemented uncertain. Furthermore, preferential flow was not observed for the finest grain size in *Katsushima et al. (2013)*, which, as shown by the black coloured areas in Fig. 6e, exists only for short periods of time in new snow. Although regimes with stable flow have been identified for soil (*DiCarlo, 2013*), using larger snow samples to investigate preferential flow in snow could exclude the possibility that finger width exceeds the snow sample size for the finest grain size class.

We consider condition 2 to be a relatively well founded approach, as the role of water entry suction in forming preferential flow was clearly identified in laboratory experiments (*Katsushima et al., 2013*) and turned out to be crucial in forming preferential flow in multi-dimensional models in agreement with laboratory experiments (*Hirashima et al., 2014*). However, also here, the exact parameterisation of water entry suction may be different for lower water influx rates.

Condition 3 may be one of the most uncertain ones. Understanding the LWC distribution in a preferential flow path cannot be achieved by the Richards equation (*DiCarlo, 2013*). The other issue is that infiltration in an initially dry porous medium is not accurately described by Richards equation. We consider the assumption we made here that water will move from preferential flow to matrix flow based on the exceedance of a threshold in saturation one of the least supported by experimental results.

The refreezing of preferential flow (condition 4) is mainly limited by knowledge about the number of preferential flow paths that are actively transporting water, which in itself is dependent on snowpack conditions. Laboratory experiments at low input rates and with initially sub-freezing snow, using detailed temperature measurements and dye-tracer to follow the wetting, may help here to develop a better understanding of the heat exchange processes between preferential flow paths and surrounding snow matrix, as a function of preferential flow area and the number density of active preferential flow paths. Results from laboratory experiments and multi-dimensional snowpack models may thereby allow to quantify the amount of refreezing of percolating melt water in flow fingers. This knowledge is of crucial importance, as it determines the efficiency of preferential flow to heat deeper layers of the snowpack. Furthermore, refreezing of preferential flow probably slows down the downward propagation of the fingers.

The term preferential flow can be interpreted ambiguously. Two phenomena are known to cause deviations from a matrix infiltration pattern: flow fingering and macropore flow. Here, we consider flow fingering purely as the result of instabilities of the wetting front, which can occur in porous media with a uniform pore space distribution. Generally the prerequisite for this effect (coarse grains and low infiltration rates) is fulfilled for snow. However, once flow fingering is occurring in snow, microstructural changes of the snow grains in preferential flow paths will change the pore space distribution to a bimodal or multi-modal one. This has its equivalent in soils in, for example, worm holes, root channels and cracks. This effect is not considered in the dual domain approach we propose, although it may have a profound impact on the efficiency of preferential flow paths. Modifications to the parameters of the preferential flow domain can be imagined to better represent a multi-modal pore space distribution. On the other hand, snow microstructure inside and around preferential flow paths may not always consist of an ice matrix where Richards equation would be a good description of water flow. However, a dual domain approach does not require both domains to be solved with Richards equation, and another description of water flow in the preferential flow domain may be more appropriate.

Our simulations have a relatively low reproduction success of observed ice layers. The sensitivity study has revealed that one factor is the delicate balance between refreezing and further percolation. This is expected to be particularly delicate in alpine snowpacks, where the cold content is low and the ice layers are often thin. For cold regions, for example the Greenland Ice Sheet, the abundance of ice layers observed in ice cores may be easier to reproduce in simulations, as microstructural transitions formed by summer melt-freeze crusts below cold new snow from the accumulation period are more easy to capture in simulations. In contrast with alpine snowpacks, where the ground heat flux often maintains melting conditions at the snowpack base, firn temperatures are generally well below freezing, and create a large refreezing capacity.

Another factor contributing to the low probability of detection is the small vertical and sometimes small horizontal scale on which ice layer formation happens in alpine snowpacks, which is difficult to capture in simulations. A correct simulation of the snow microstructure is thereby a prerequisite for simulating ice layer formation, although it is difficult to achieve. As an example, buried surface hoar may provide a marked microstructural transition on which liquid water may pond and build ice layers. Whether or not the simulation is able to simulate correctly the burial of surface hoar, contributes to the failure or success in reproducing ice layers. Such a failure or success will remain throughout the rest of the snow season.

6 Conclusions

We proposed a dual domain approach for modelling liquid water flow in snow, which separates the pore space in a part that is representing matrix flow and a part that is representing preferential flow. This dual domain approach for physics based snowpack models is able to simulate preferential flow paths such that, by using two tuning parameters, a better agreement with the onset of snowpack runoff can be achieved. The difference between the first modelled and measured 20 mm w.e. cumulative snowpack runoff decreased from approximately 8 days too late to 3 days too early. Furthermore, preferential flow ponding on microstructural transitions inside the snowpack and subsequent spreading in the matrix flow domain can simulate the otherwise lacking formation of dense layers by the model. Around 20 % of observed ice layers in the field over 16 snow seasons were correctly simulated by the model in the form of a layer exceeding a dry snow density of 700 kg m^{-3} . We showed that a dual domain approach is able to provide a physics based description of preferential flow and ice layer formation that is corresponding to findings in laboratory and field experiments. However, the formulation has two parameters that were calibrated for this study. Although we do not resolve individual flow paths, as is done in multi-dimensional snowpack models, a dual domain approach can quantify the net effect of preferential flow on a snowpack in a 1-D snowpack model with much lower computational costs than multi-dimensional models and only marginally larger computational cost compared to 1-D non-multidomain models.

Acknowledgements. Funding for this research was provided by the Swiss National Science Foundation (NSF), grant number 200021E-160667. We thank the many employees of the WSL Institute for Snow and Avalanche Research SLF involved in taking the bi-weekly snow profiles at the Weissfluhjoch. Meteorological driving data for the SNOWPACK model as well as the bi-weekly snow profiles are accessible via doi 10.16904/1 (*WSL Institute for Snow and Avalanche Research SLF*, 2015-09-29) and 10.16904/2 (*WSL Institute for Snow and Avalanche Research SLF*, 2015), respectively. The SNOWPACK model is available under a LGPLv3 license at <http://models.slf.ch>. The version used in this study corresponds to revision 1028 of /branches/dev/pref_flow.

References

- Albert, M., G. Koh, and F. Perron (1999), Radar investigations of melt pathways in a natural snowpack, *Hydrol. Proc.*, 13(18), 2991–3000, doi:10.1002/(SICI)1099-1085(19991230)13:18<2991::AID-HYP10>3.0.CO;2-5.
- Avanzi, F., H. Hirashima, S. Yamaguchi, T. Katsushima, and C. De Michele (2015), Laboratory-based observations of capillary barriers and preferential flow in layered snow, *Cryosphere Discuss.*, 9(6), 6627–6659, doi:10.5194/tcd-9-6627-2015.
- Bartelt, P., and M. Lehning (2002), A physical SNOWPACK model for the Swiss avalanche warning Part I: Numerical model, *Cold Reg. Sci. Technol.*, 35(3), 123–145, doi:10.1016/S0165-232X(02)00074-5.
- Brun, E., P. David, M. Sudul, and G. Brunot (1992), A numerical model to simulate snow-cover stratigraphy for operational avalanche forecasting, *J. Glaciol.*, 38(128), 13–22.
- Calonne, N., C. Geindreau, F. Flin, S. Morin, B. Lesaffre, S. Rolland du Roscoat, and P. Charrier (2012), 3-D image-based numerical computations of snow permeability: links to specific surface area, density, and microstructural anisotropy, *Cryosphere*, 6(5), 939–951, doi:10.5194/tc-6-939-2012.
- Colbeck, S. (1979), Water flow through heterogeneous snow, *Cold Reg. Sci. Technol.*, 1(1), 37–45, doi:10.1016/0165-232X(79)90017-X.
- Colbeck, S. C. (1991), The layered character of snow covers, *Rev. Geophys.*, 29(1), 81–96, doi:10.1029/90RG02351.
- de la Peña, S., I. M. Howat, P. W. Nienow, M. R. van den Broeke, E. Mosley-Thompson, S. F. Price, D. Mair, B. Noël, and A. J. Sole (2015), Changes in the firn structure of the western Greenland Ice Sheet caused by recent warming, *Cryosphere*, 9(3), 1203–1211, doi:10.5194/tc-9-1203-2015.
- DiCarlo, D. A. (2013), Stability of gravity-driven multiphase flow in porous media: 40 years of advancements, *Water Resour. Res.*, 49(8), 4531–4544, doi:10.1002/wrcr.20359.
- Eiriksson, D., M. Whitson, C. H. Luce, H. P. Marshall, J. Bradford, S. G. Benner, T. Black, H. Hetrick, and J. P. McNamara (2013), An evaluation of the hydrologic relevance of lateral flow in snow at hillslope and catchment scales, *Hydrol. Proc.*, 27(5), 640–654, doi:10.1002/hyp.9666.
- Fierz, C., R. Armstrong, Y. Durand, P. Etchevers, E. Greene, D. McClung, K. Nishimura, P. Satyawali, and S. Sokratov (2009), The International Classification for Seasonal Snow on the Ground (ICSSG), *Tech. rep.*, IHP-VII Technical Documents in Hydrology No. 83, IACS Contribution No. 1, UNESCO-IHP, Paris.
- Glass, R. J., J. Y. Parlange, and T. S. Steenhuis (1989a), Wetting front instability 1. theoretical discussion and dimensional analysis, *Water Resour. Res.*, 25(6), 1187–1194, doi:10.1029/WR025i006p01187.
- Glass, R. J., J. Y. Parlange, and T. S. Steenhuis (1989b), Wetting front instability 2. experimental determination of relationships between system parameters and two-dimensional unstable flow field behavior in initially dry porous media, *Water Resour. Res.*, 25(6), 1195–1207, doi:10.1029/WR025i006p01195.
- Hammonds, K., R. Lieb-Lappen, I. Baker, and X. Wang (2015), Investigating the thermophysical properties of the ice-snow interface under a controlled temperature gradient: Part I: Experiments & Observations, *Cold Reg. Sci. Technol.*, 120, 157–167, doi:10.1016/j.coldregions.2015.09.006.
- Hirashima, H., S. Yamaguchi, and T. Katsushima (2014), A multi-dimensional water transport model to reproduce preferential flow in the snowpack, *Cold Reg. Sci. Technol.*, 108, 80–90, doi:10.1016/j.coldregions.2014.09.004.
- Humphrey, N. F., J. T. Harper, and W. T. Pfeffer (2012), Thermal tracking of meltwater retention in Greenland’s accumulation area, *J. Geophys. Res.*, 117(F1), doi:10.1029/2011JF002083.

- Illangasekare, T. H., R. J. Walter, Jr., M. F. Meier, and W. T. Pfeffer (1990), Modeling of meltwater infiltration in subfreezing snow, *Water Resour. Res.*, 26(5), 1001–1012, doi:10.1029/WR026i005p01001.
- Katsushima, T., T. Kumakura, and Y. Takeuchi (2009), A multiple snow layer model including a parameterization of vertical water channel process in snowpack, *Cold Reg. Sci. Technol.*, 59(2–3), 143–151, doi:10.1016/j.coldregions.2009.09.002, international Snow Science Workshop (ISSW) 2008.
- Katsushima, T., S. Yamaguchi, T. Kumakura, and A. Sato (2013), Experimental analysis of preferential flow in dry snowpack, *Cold Reg. Sci. Technol.*, 85, 206–216, doi:10.1016/j.coldregions.2012.09.012.
- Kattelmann, R. (1985), Macropores in snowpacks of Sierra Nevada, *Ann. Glaciol.*, 6, 272–273.
- Kattelmann, R. (2000), Snowmelt lysimeters in the evaluation of snowmelt models, *Ann. Glaciol.*, 31(1), 406–410, doi:10.3189/172756400781820048.
- Lehning, M., P. Bartelt, B. Brown, T. Russi, U. Stöckli, and M. Zimmerli (1999), SNOWPACK calculations for avalanche warning based upon a new network of weather and snow stations, *Cold Reg. Sci. Technol.*, 30(1–3), 145–157, doi:10.1016/S0165-232X(99)00022-1.
- Lehning, M., P. Bartelt, B. Brown, C. Fierz, and P. Satyawali (2002a), A physical SNOWPACK model for the Swiss avalanche warning Part II: Snow microstructure, *Cold Reg. Sci. Technol.*, 35(3), 147–167, doi:10.1016/S0165-232X(02)00073-3.
- Lehning, M., P. Bartelt, B. Brown, and C. Fierz (2002b), A physical SNOWPACK model for the Swiss avalanche warning Part III: Meteorological forcing, thin layer formation and evaluation, *Cold Reg. Sci. Technol.*, 35(3), 169–184, doi:10.1016/S0165-232X(02)00072-1.
- Machguth, H., M. MacFerrin, D. van As, J. E. Box, C. Charalampidis, W. Colgan, R. S. Fausto, H. A. J. Meijer, E. Mosley-Thompson, and R. S. W. van de Wal (2016), Greenland meltwater storage in firn limited by near-surface ice formation, *Nature Clim. Change*, 6(4), 390–393, doi:10.1038/nclimate2899.
- Marsh, P. (1988), Flow fingers and ice columns in a cold snow cover, in *Proceedings of the 56th Annual Western Snow Conference*, Western Snow Conference, Kalispell, Montana.
- Marsh, P. (1999), Snowcover formation and melt: recent advances and future prospects, *Hydrol. Proc.*, 13(14–15), 2117–2134, doi:10.1002/(SICI)1099-1085(199910)13:14/15<2117::AID-HYP869>3.0.CO;2-9.
- Marsh, P., and M.-K. Woo (1984), Wetting front advance and freezing of meltwater within a snow cover: 2. A simulation model, *Water Resour. Res.*, 20(12), 1865–1874, doi:10.1029/WR020i012p01865.
- Marsh, P., and M.-K. Woo (1985), Meltwater movement in natural heterogeneous snow covers, *Water Resour. Res.*, 21(11), 1710–1716, doi:10.1029/WR021i011p01710.
- McGurk, B. J., and P. Marsh (1995), Flow-finger continuity in serial thick-sections in a melting sierran snowpack, in *Biogeochemistry of Seasonally Snow-Covered Catchments (Proceedings of a Boulder Symposium, July 1995)*, IAHS publ. no. 228.
- Pfeffer, W. T., and N. F. Humphrey (1998), Formation of ice layers by infiltration and refreezing of meltwater, *Ann. Glaciol.*, 26, 83–91.
- Pfeffer, W. T., M. F. Meier, and T. H. Illangasekare (1991), Retention of Greenland runoff by refreezing: Implications for projected future sea level change, *J. Geophys. Res.*, 96(C12), 22,117–22,124, doi:10.1029/91JC02502.
- Phillips, M., A. Haberhorn, D. Draebing, M. Krautblatter, H. Rhyner, and R. Kenner (2016), Seasonally intermittent water flow through deep fractures in an Alpine Rock Ridge: Gemsstock, Central Swiss Alps, *Cold Reg. Sci. Technol.*, 125, 117–127, doi:10.1016/j.coldregions.2016.02.010.
- Rees, A., J. Lemmetyinen, C. Derksen, J. Pulliainen, and M. English (2010), Observed and modelled effects of ice lens formation on passive microwave brightness temperatures over snow covered tundra, *Remote Sens. Environ.*, 114(1), 116–126, doi:10.1016/j.rse.2009.08.013.

- Rössler, O., P. Froidevaux, U. Börst, R. Rickli, O. Martius, and R. Weingartner (2014), Retrospective analysis of a nonforecasted rain-on-snow flood in the Alps – a matter of model limitations or unpredictable nature?, *Hydrol. Earth Syst. Sci.*, 18(6), 2265–2285, doi:10.5194/hess-18-2265-2014.
- Roy, A., A. Royer, O. St-Jean-Rondeau, B. Montpetit, G. Picard, A. Mavrovic, N. Marchand, and A. Langlois (2016), Microwave snow emission modeling uncertainties in boreal and subarctic environments, *Cryosphere*, 10(2), 623–638, doi:10.5194/tc-10-623-2016.
- Schneebeli, M. (1995), Development and stability of preferential flow paths in a layered snowpack, in *Biogeochemistry of Seasonally Snow-Covered Catchments (Proceedings of a Boulder Symposium July 1995)*, edited by K. Tonnessen, M. Williams, and M. Tranter, p. 89–95, AHS Publ. no. 228.
- Schneebeli, M., and J. Johnson (1998), A constant-speed penetrometer for high-resolution snow stratigraphy, *Ann. Glaciol.*, 26, 107–111.
- Singh, P., G. Spitzbart, H. Hübl, and H. Weinmeister (1997), Hydrological response of snowpack under rain-on-snow events: a field study, *J. Hydrol.*, 202(1–4), 1–20, doi:10.1016/S0022-1694(97)00004-8.
- Surfleet, C. G., and D. Tullos (2013), Variability in effect of climate change on rain-on-snow peak flow events in a temperate climate, *J. Hydrol.*, 479, 24–34, doi:10.1016/j.jhydrol.2012.11.021.
- Vikhamar-Schuler, D., I. Hanssen-Bauer, T. Schuler, S. Mathiesen, and M. Lehning (2013), Use of a multilayer snow model to assess grazing conditions for reindeer, *Ann. Glaciol.*, 54(62), 214–226, doi:10.3189/2013AoG62A306.
- Watts, T., N. Rutter, P. Toose, C. Derksen, M. Sandells, and J. Woodward (2016), Brief communication: Improved measurement of ice layer density in seasonal snowpacks, *Cryosphere*, 10(5), 2069–2074, doi:10.5194/tc-10-2069-2016.
- Wever, N., C. Fierz, C. Mitterer, H. Hirashima, and M. Lehning (2014a), Solving Richards Equation for snow improves snowpack meltwater runoff estimations in detailed multi-layer snowpack model, *Cryosphere*, 8(1), 257–274, doi:10.5194/tc-8-257-2014.
- Wever, N., T. Jonas, C. Fierz, and M. Lehning (2014b), Model simulations of the modulating effect of the snow cover in a rain-on-snow event, *Hydrol. Earth Syst. Sci.*, 18(11), 4657–4669, doi:10.5194/hess-18-4657-2014.
- Wever, N., L. Schmid, A. Heilig, O. Eisen, C. Fierz, and M. Lehning (2015), Verification of the multi-layer SNOWPACK model with different water transport schemes, *Cryosphere*, 9(6), 2271–2293, doi:10.5194/tc-9-2271-2015.
- Wever, N., C. Vera Valero, and C. Fierz (2016), Assessing wet snow avalanche activity using detailed physics based snowpack simulations, *Geophys. Res. Lett.*, 43(11), 5732–5740, doi:10.1002/2016GL068428.
- Williams, M. W., M. Rikkers, and W. T. Pfeffer (2000), Ice column and frozen rills in a warm snowpack, Green Lakes Valley, Colorado, U.S.A., *Nord. Hydrol.*, 31(3), 169–186.
- Willmott, C. J. (1981), On the validation of models, *Phys. Geogr.*, 2(2), 184–194, doi:10.1080/02723646.1981.10642213.
- WSL Institute for Snow and Avalanche Research SLF (2015), *Manual bi-weekly snow profiles from Weissfluhjoch, Davos, Switzerland*, doi:10.16904/2.
- WSL Institute for Snow and Avalanche Research SLF (2015-09-29), *Meteorological and snowpack measurements from Weissfluhjoch, Davos, Switzerland*, 1, doi:10.16904/1, dataset.
- Würzer, S., T. Jonas, N. Wever, and M. Lehning (2016a), Influence of initial snowpack properties on runoff formation during rain-on-snow events, *J. Hydrometeor.*, 17(6), 1801–1815, doi:10.1175/JHM-D-15-0181.1.
- Würzer, S., N. Wever, R. Juras, M. Lehning, and T. Jonas (2016b), Modeling liquid water transport in snow under rain-on-snow conditions – considering preferential flow, *Hydrol. Earth Syst. Sci. Discuss.*, doi:10.5194/hess-2016-351.
- Yamaguchi, S., K. Watanabe, T. Katsushima, A. Sato, and T. Kumakura (2012), Dependence of the water retention curve of snow on snow characteristics, *Ann. Glaciol.*, 53(61), 6–12, doi:10.3189/2012AoG61A001.

- Ye, H., D. Yang, and D. Robinson (2008), Winter rain on snow and its association with air temperature in northern Eurasia, *Hydrol. Proc.*, 22(15), 2728–2736, doi:10.1002/hyp.7094.
- Zambrano-Bigiarini, M. (2014), *hydroGOF: Goodness-of-fit functions for comparison of simulated and observed hydrological time series*, r package version 0.3-8, <https://CRAN.R-project.org/package=hydroGOF>.

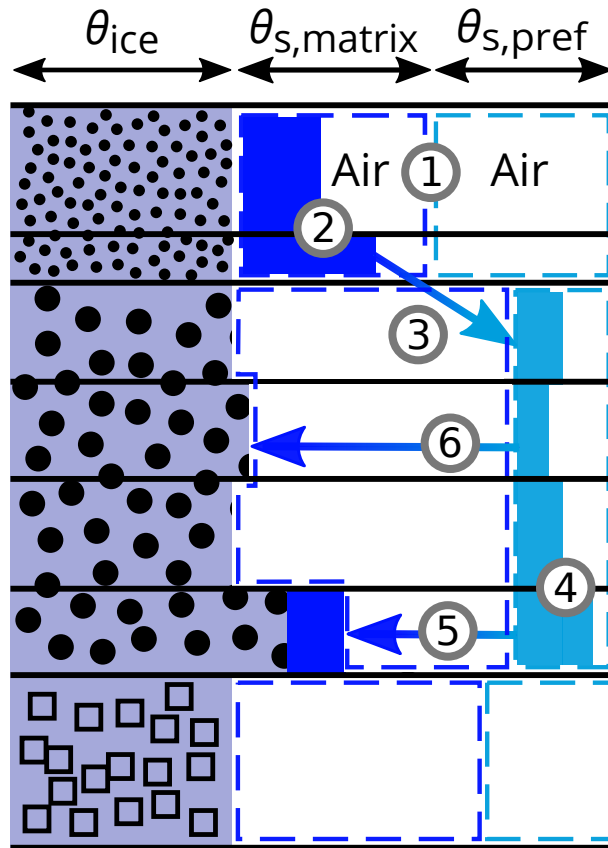


Figure 1. Schematic overview of the dual domain implementation for the SNOWPACK model, in which the pore space that can be occupied by liquid water is separated into a part for matrix flow ($\theta_{s,matrix}$) and a part representing preferential flow ($\theta_{s,pref}$). The numbers refer to processes described in the text.

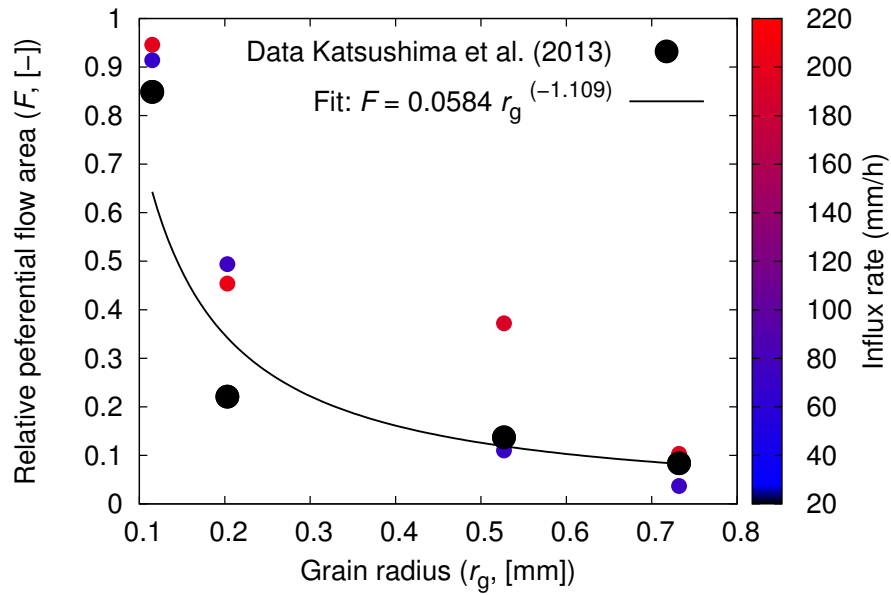


Figure 2. Relationship of the area involved in preferential flow as a function of grain radius. Data points represent laboratory experiments by *Katsushima et al. (2013)*, presented quantitatively by *Hirashima et al. (2014)*. Data points are coloured based on the water influx rate used in the experiments. The large black dots denote the data points used for determining the fit (solid line), corresponding to the lowest influx rate per grain size class.

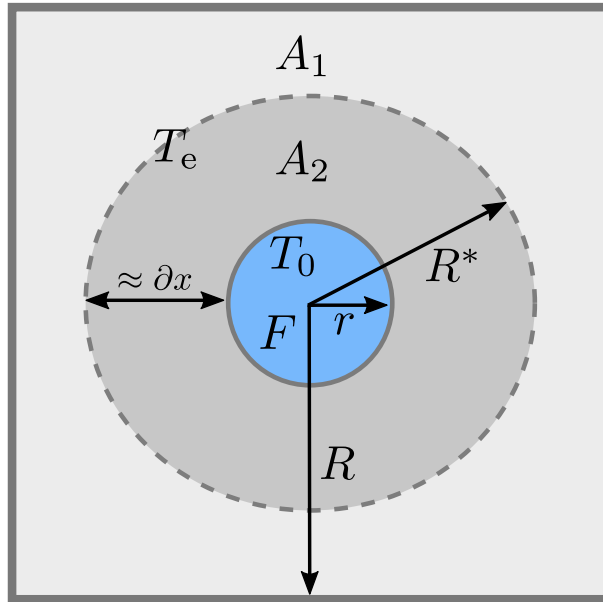


Figure 3. Schematic representation of a preferential flow path with radius r and surface F inside a 1 m^2 snowpack (i.e., $R = 0.5 \text{ m}$), seen from above (not to scale), to approximate ∂x . The preferential flow path is assumed to be at melting temperature T_0 , the rest of the snowpack at temperature T_e . R^* is the radius such that surface areas A_1 and A_2 are equal. When assuming a linear temperature gradient, T_e is found at distance R^* .

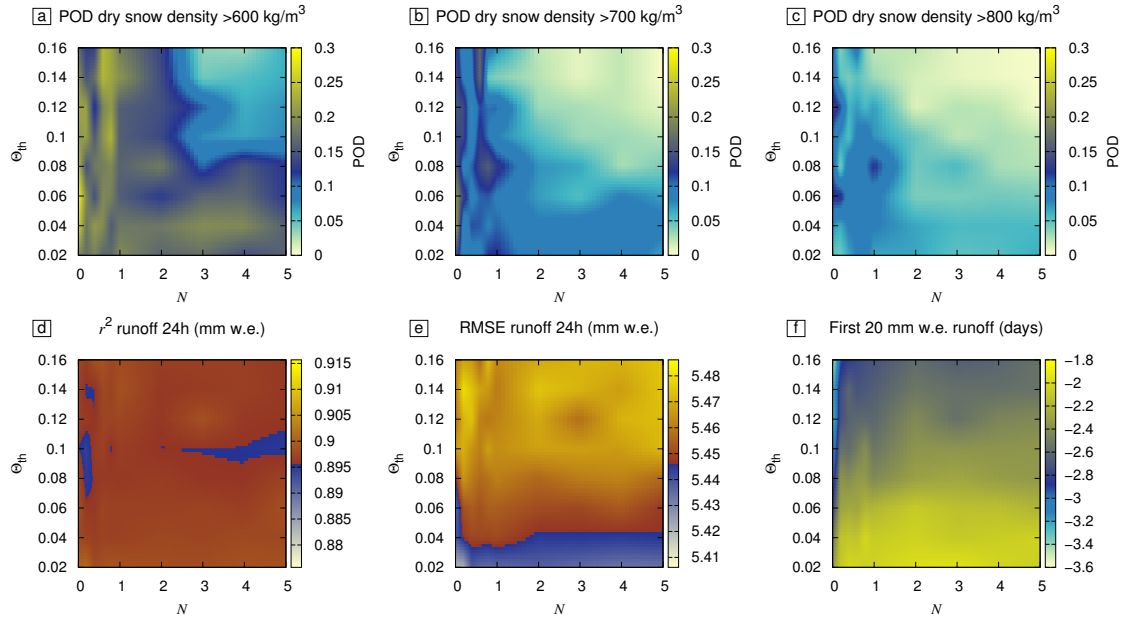


Figure 4. Interpolated results of the sensitivity study for the parameters N and Θ_{th} for the probability of detection (POD) when modelled dry snow density exceeds 600 kg m^{-3} (a), 700 kg m^{-3} (b), or 800 kg m^{-3} (c) within 20 cm of the observed ice layer. For runoff, the r^2 for daily sums of runoff (d), the RMSE error for daily sums of runoff (e) and the number of days difference between modelled and measured passage of 20 mm w.e. since March, 1 of each snow season (f). The jump in colour scale from blue to red in (d) and (e) mark the score achieved with matrix flow only.

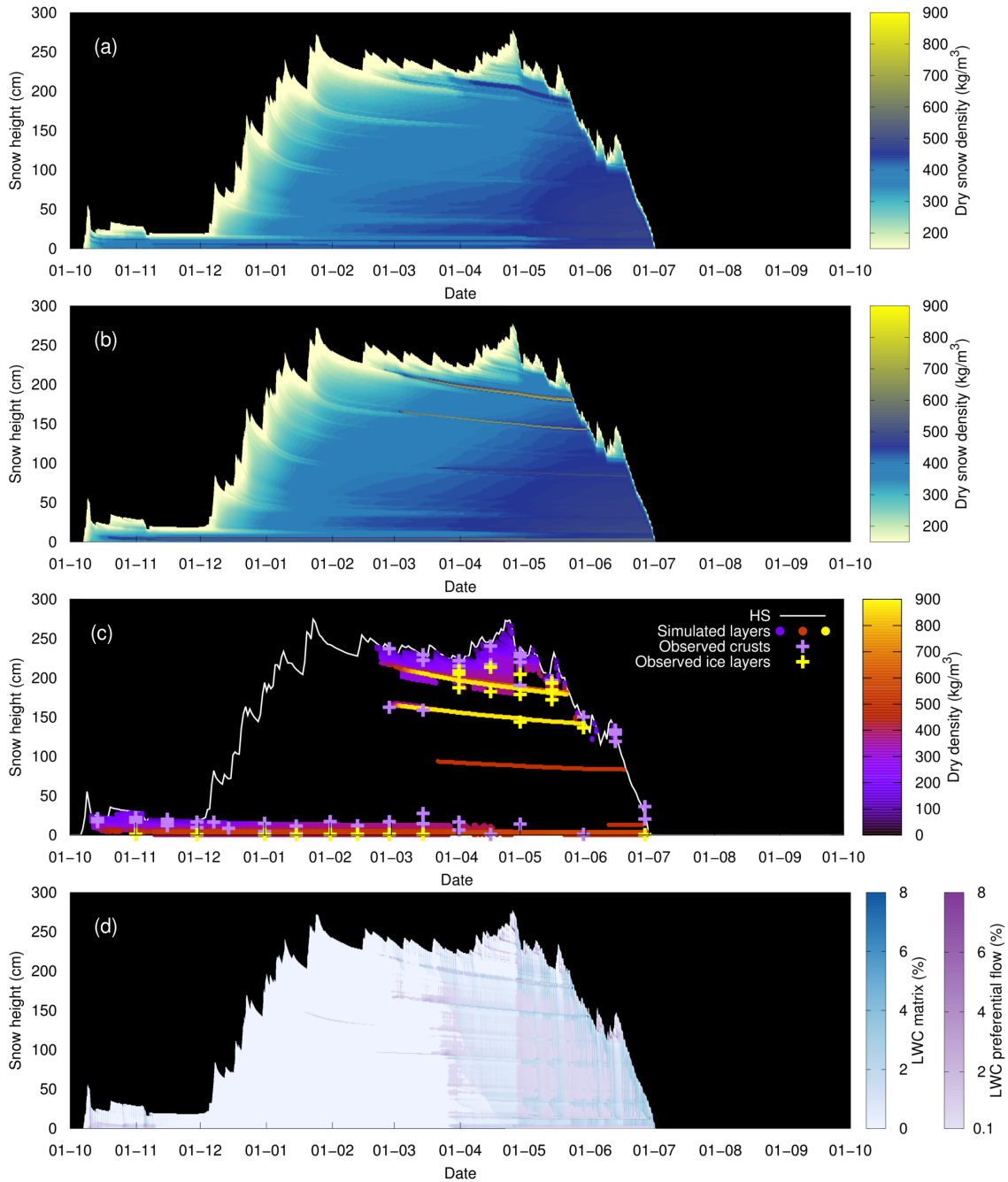


Figure 5. Dry snow density without considering preferential flow (a) and with preferential flow using high resolution simulations (b), validation with field observations (c) and liquid water content in the matrix and preferential flow domain for the simulation with preferential flow (d), for snow season 2012. In (c), modelled layers are shown when they are either a melt-freeze crust, or have a dry snow density exceeding 500 kg m^{-3} . For visibility, values of LWC in preferential flow below 0.1 % are ignored in (d).

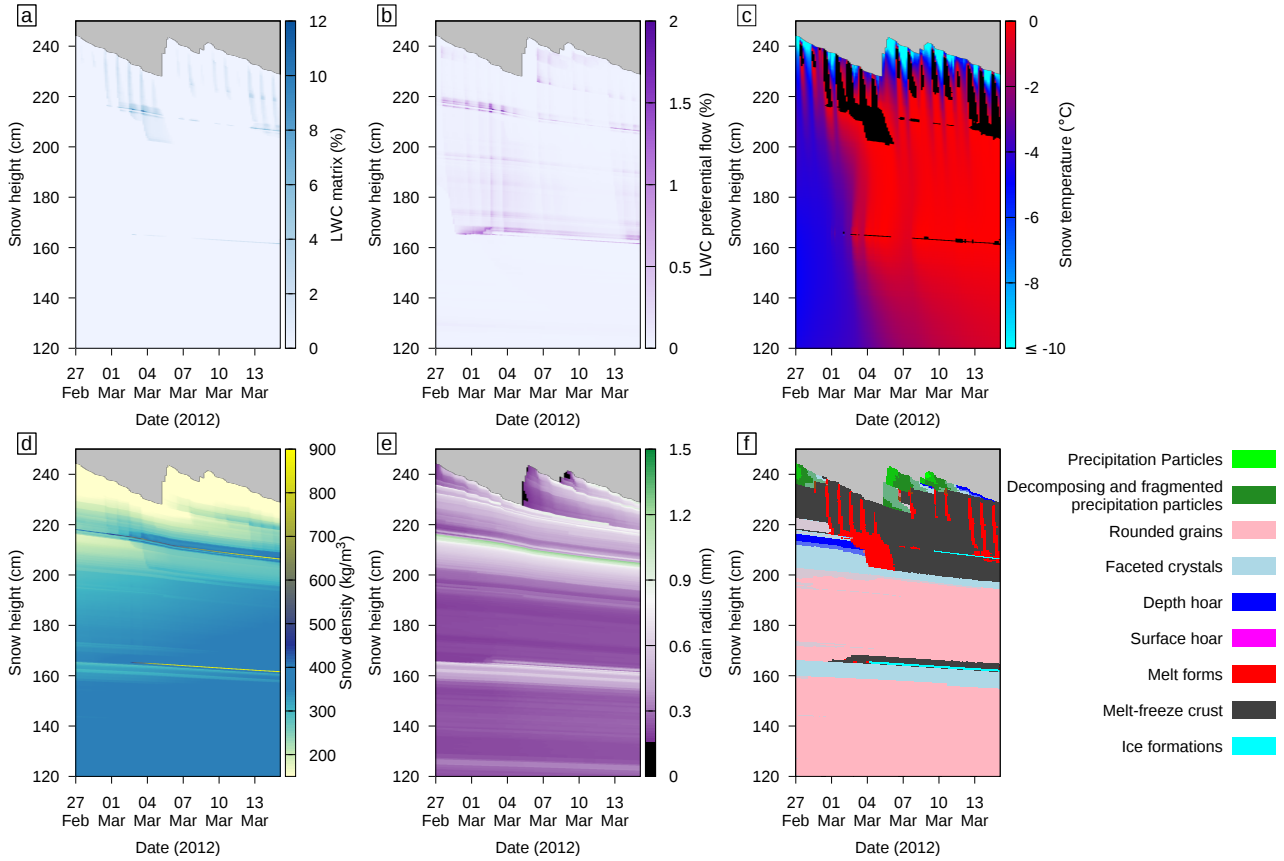


Figure 6. LWC in matrix domain (a), LWC in preferential flow domain (b), snow temperature (c), snow density (d), grain radius (e) and grain shape (f), depicting a detail of Fig. 5. Only the upper part of the snowpack is shown for the period February 27 to March 15. In (c), snow at melting temperature is coloured black to highlight wet parts, in (e), grain radii smaller than 0.16 mm are coloured black, denoting the smallest grain size class used in *Katsushima et al.* (2013), and in (f), ice formations are defined as modelled dry snow density exceeding 700 kg/m^3 .

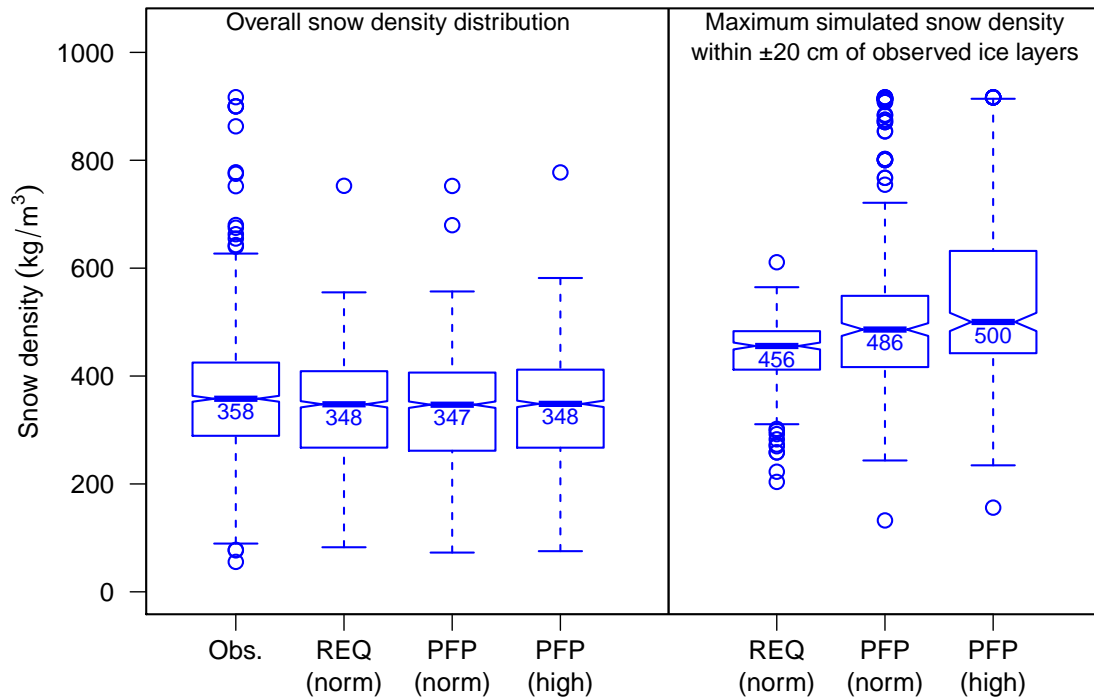


Figure 7. Box and whisker plot showing the distribution of snow density from observations (obs), simulations with Richards equation (REQ) and simulations with the dual domain approach to describe preferential flow (PFP). On the left, simulated snow density represents an aggregated snow density over multiple model layers to match the measured layer thickness. On the right, snow density of an individual model layer is shown. Boxes represent inter-quartile ranges (25th to 75th percentiles), thick horizontal bars in each box denote the median (50th percentile), its value shown directly below the bar. Whiskers (vertical lines and thin horizontal bars) represent the highest and lowest value within 1.5 times the inter-quartile range above the upper or below the lower quartile, respectively. Notches are drawn at ± 1.58 times the inter-quartile range divided by the square root of the number of data points. Outliers are shown as individual dots.

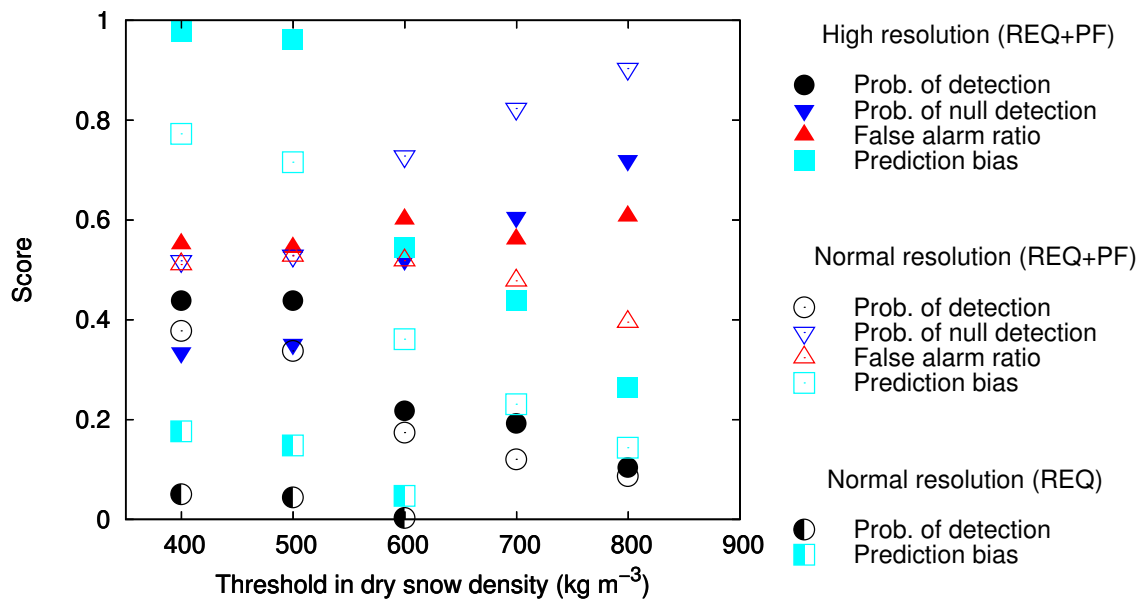


Figure 8. Contingency statistics as a function of threshold in dry snow density that defines an ice layer in the simulations, for both normal and high resolution simulations including preferential flow (REQ+PF) and normal resolution simulations using Richards equation only (REQ).

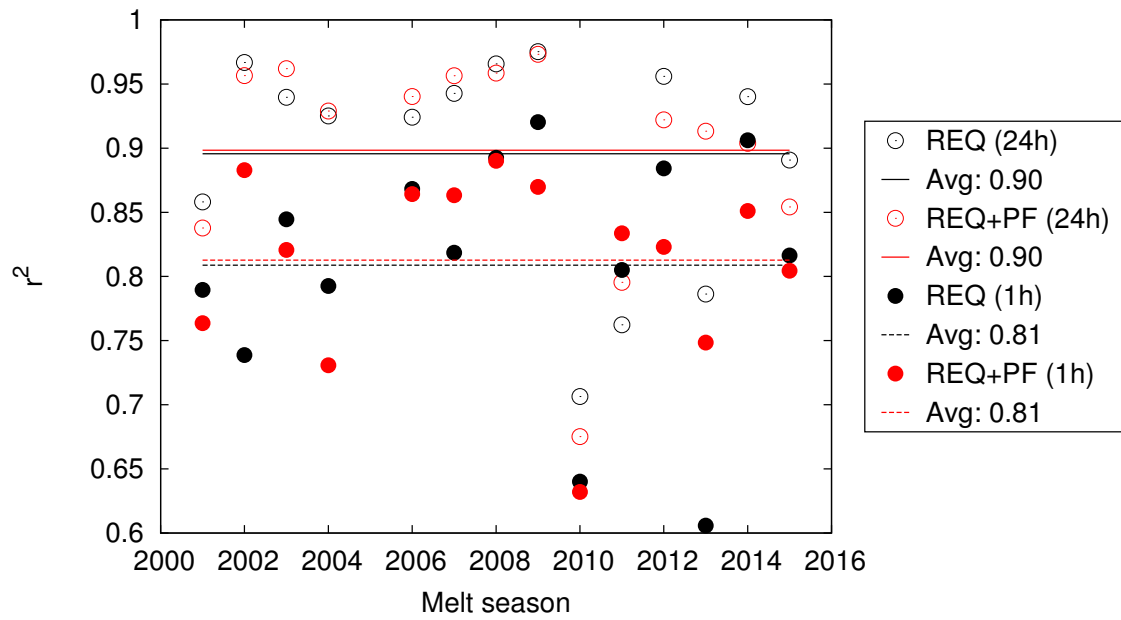


Figure 9. r^2 for both hourly and daily snowpack runoff over the period March 1 to May 31 for each snow season.

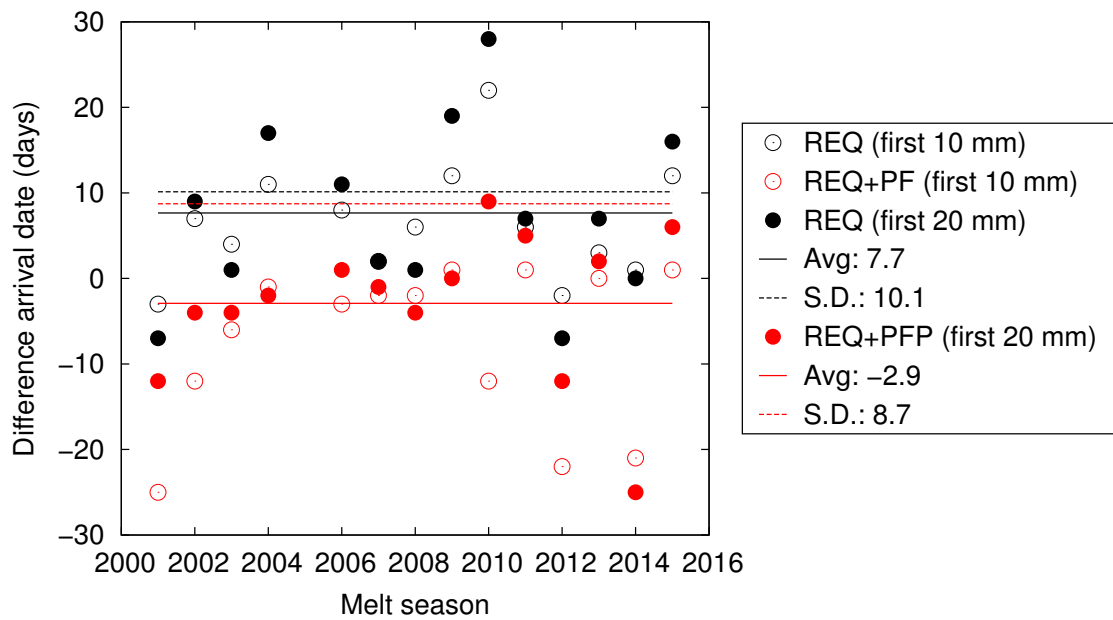


Figure 10. Difference (in days) between modelled and measured first 20 mm w.e. cumulative seasonal snowpack runoff (negative values denote modelled runoff is earlier than measured runoff).